Supporting Information

Pt_1-O_4 as active sites boosting CO oxidation via a non-classical MvK mechanism

Yang Lou[1,2,*], Yongping Zheng[3,*], Wenyi Guo[1], Jingyue Liu[2]*

[1]Department of Physics, Arizona State University, Tempe, Arizona 85287, United States

[2]International Joint Research Center for Photoresponsive Molecules and Materials, Key Laboratory of Synthetic and Biological Colloids, Ministry of Education, School of Chemical and Material Engineering, Jiangnan University, Wuxi, Jiangsu 214122, China

[3]Functional Thin Films Research Center, Shenzhen Institutes of Advanced Technology, Chinese Academy of Sciences, Shen-zhen, 518055, China

**Corresponding author: yang.lou@jiangnan.edu.cn; yp.zheng@siat.ac.cn; jingyue.liu@asu.edu.*

Contents:

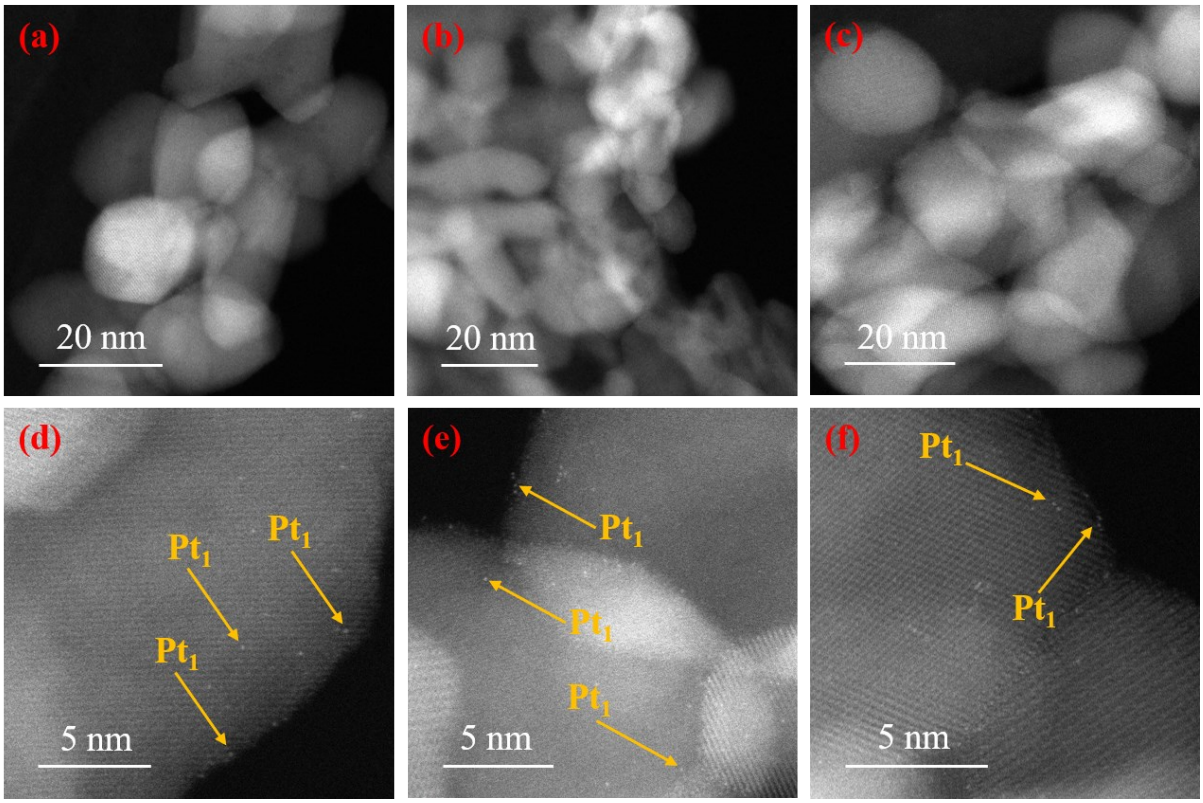

Figure S1 Low-magnification and high-magnification aberration-corrected HAADF-STEM images of fresh Pt_1/Fe_2O_3 SAC.

As shown in the low-magnification images (a-c), there are no Pt particles present in the fresh Pt_1/Fe_2O_3 SAC. Any Pt particles or clusters should appear as bright dots in HAADF images due to the strong Z-contract. High-magnification images (d-f) confirm the presence of single Pt species distributed on the surfaces of the Fe_2O_3 crystallites. Based on the HAADF-STEM images, we concluded that the fresh Pt_1/Fe_2O_3 SAC contains only isolated single Pt_1 atoms without the presence of any Pt clusters or particles.

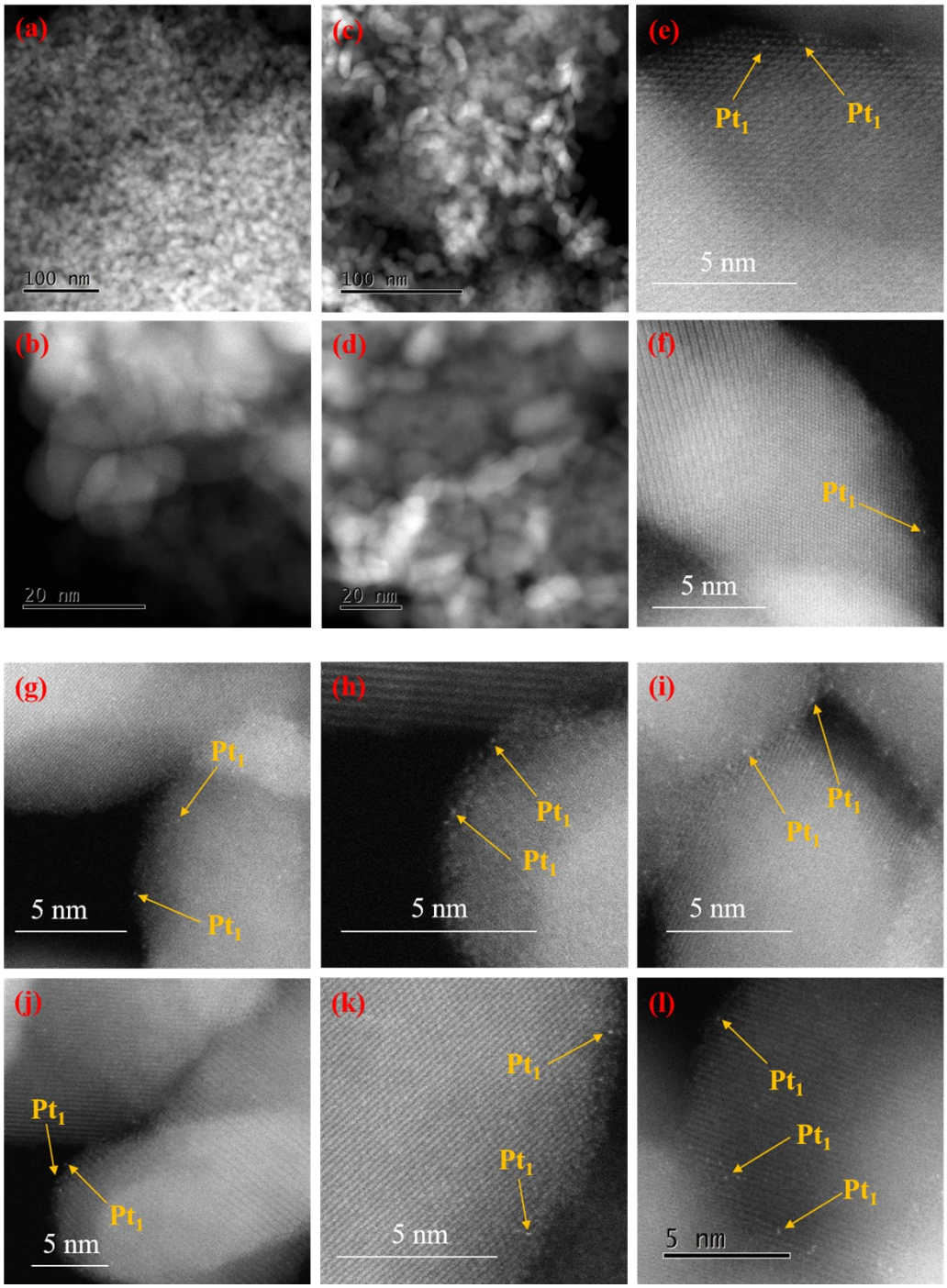

Figure S2 Low-magnification and high-magnification aberration-corrected HAADF-STEM images of used Pt_1/Fe_2O_3 SAC.

As shown in the low-magnification images (a-d), there are no Pt particles present in the used Pt_1/Fe_2O_3 SAC. High-magnification images (e-l), however, confirmed the presence of single Pt species on the Fe_2O_3 crystallites after the catalytic reaction. Based on the HAADF-STEM images, we concluded that the Pt_1 atoms did not sinter into clusters or particles during the catalytic evaluations. Such data assures that the measured catalytic activity originated from the Pt_1 atoms rather than the Pt clusters or particles.

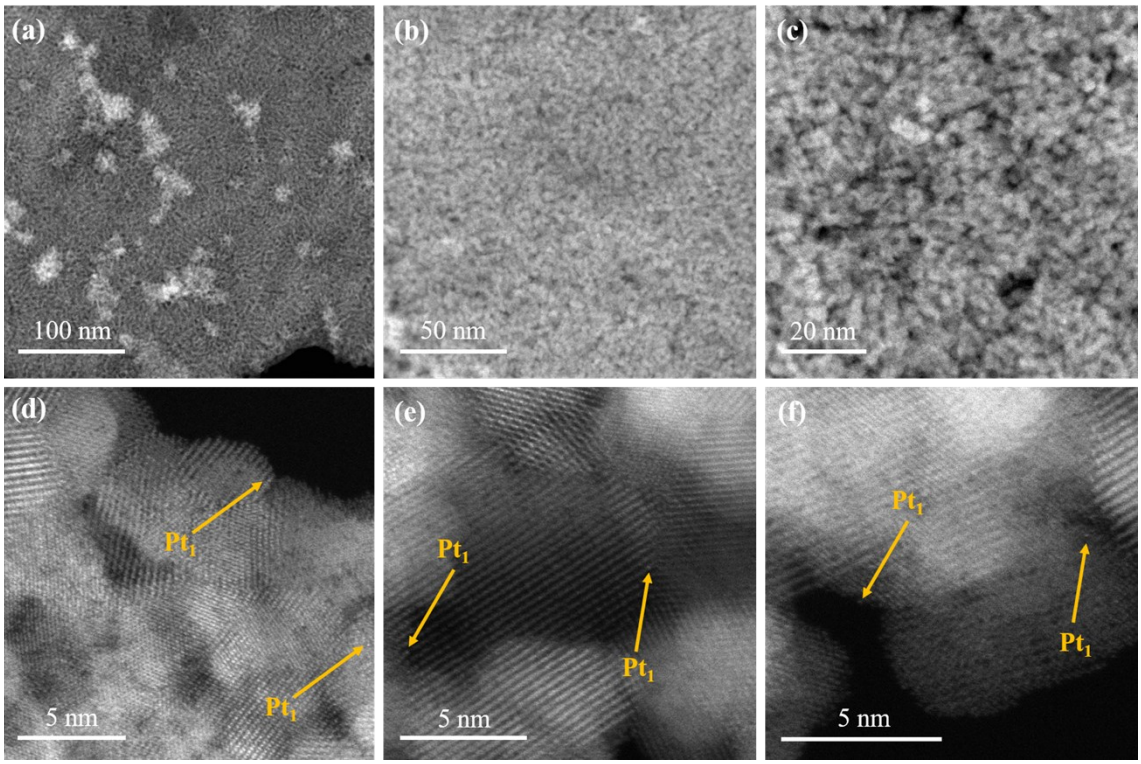

Figure S3 Low-magnification and high-magnification aberration-corrected HAADF-STEM images of fresh Pt_1/CeO_2 SAC.

As shown in the low-magnification images (a-c), there are no Pt particles present in the fresh Pt_1/CeO_2 SAC. High-magnification images (d-f) confirmed the presence of single Pt species in the fresh Pt_1/CeO_2 SAC. Based on the HAADF-STEM images, we concluded that the as-synthesized Pt_1/CeO_2 SAC contains only Pt_1 atoms without the presence of any Pt clusters or particles.

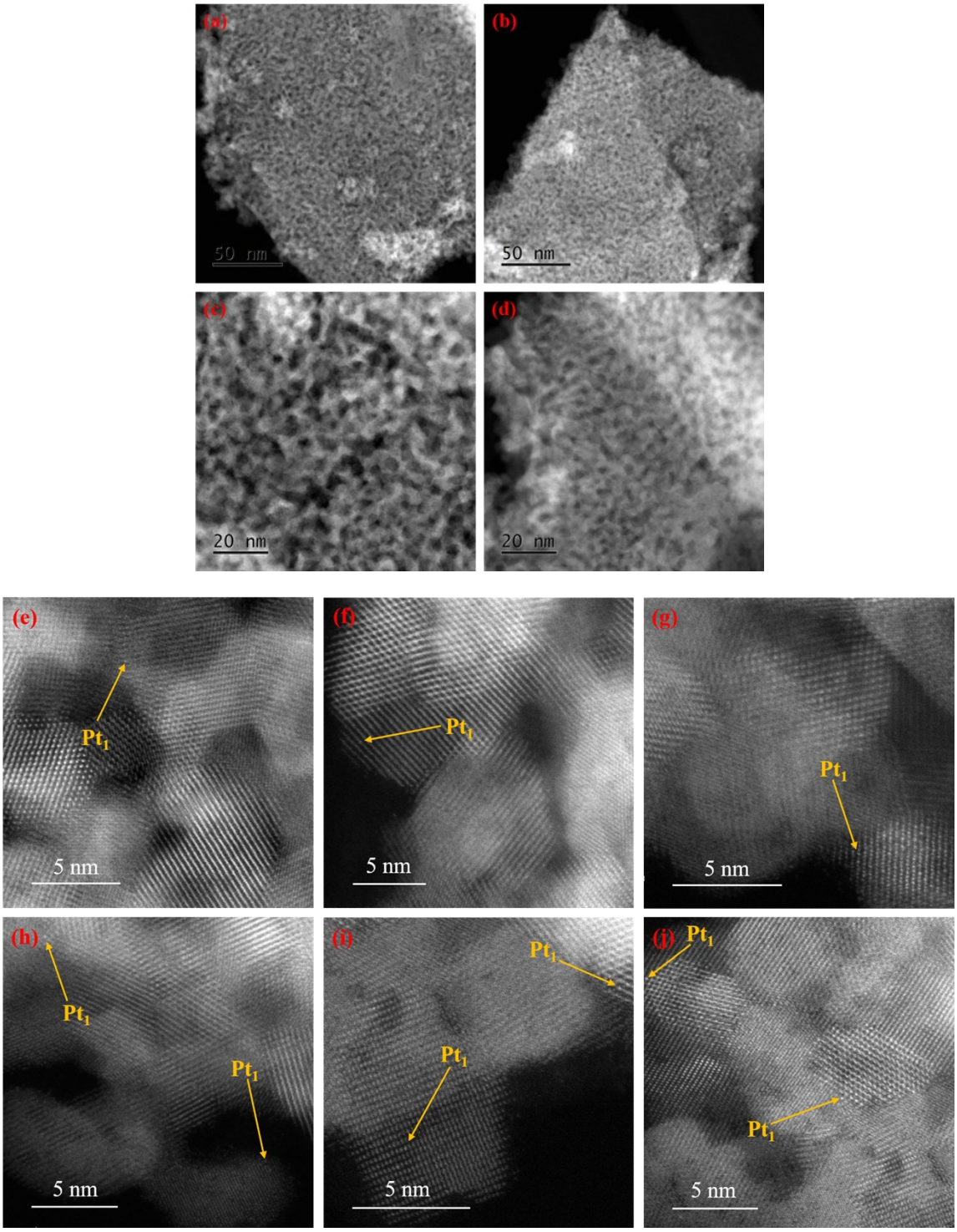

Figure S4 Low-magnification and high-magnification aberration-corrected HAADF-STEM images of used Pt_1/CeO_2 SAC.

As shown in the low-magnification images (a-d), there are no Pt particles or clusters present in the used Pt_1/CeO_2 SAC. High-magnification images (e-j) from different regions of the sample confirmed the presence of single Pt species after the catalytic reaction. Based on the HAADF-STEM images, we concluded that under the reaction condition, the Pt_1/CeO_2 SAC contained only Pt_1 atoms, which assures that the measured catalytic activity originated from the Pt_1 atoms rather than the Pt clusters or particles.

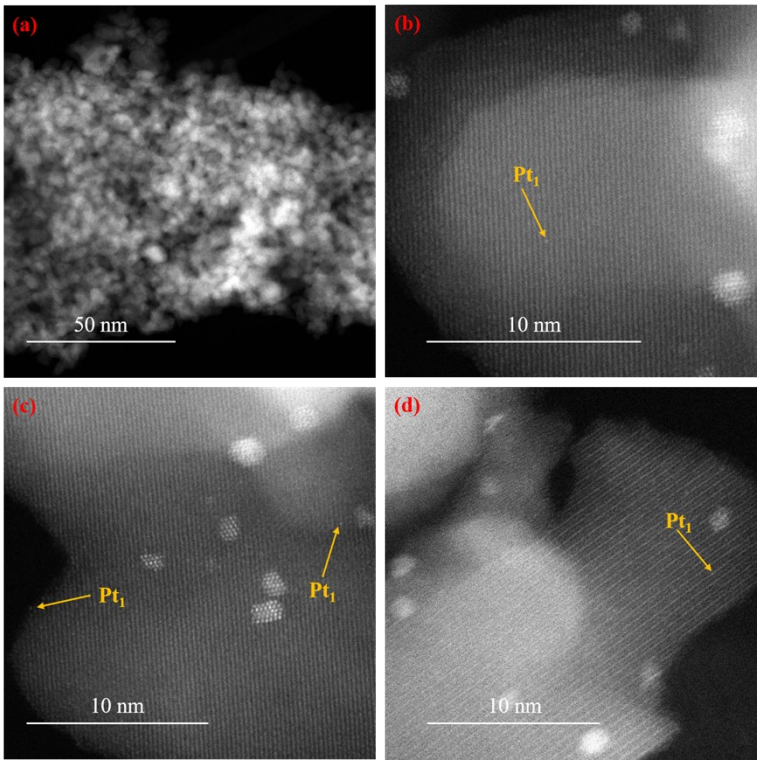
(a)
50 nm
(b)
Pt1
10 nm
(c)
Pt1
Pt1
10 nm
(d)
Pt1
10 nm

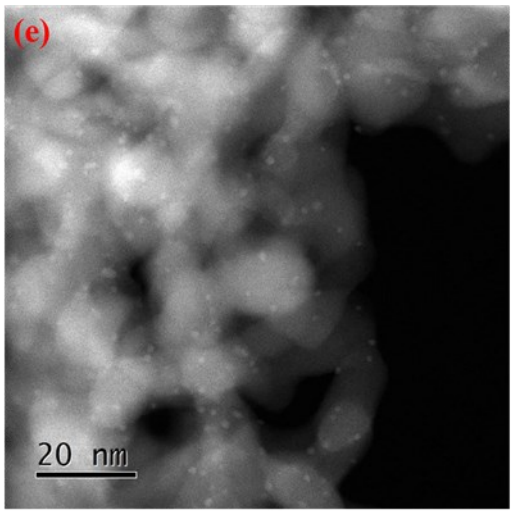
(e)
20 nm

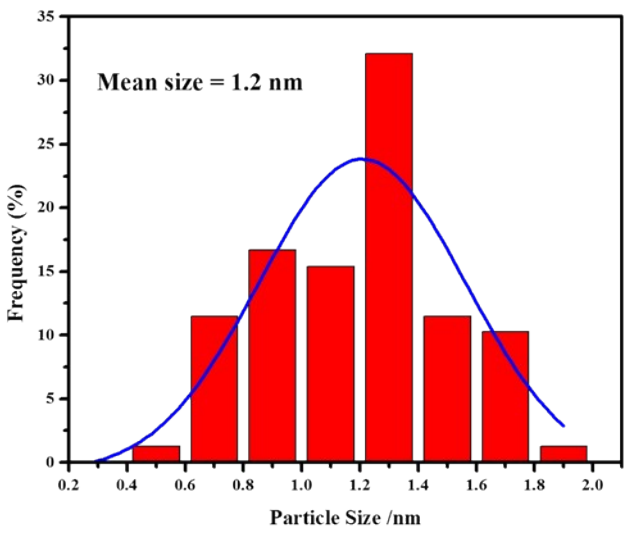
Mean size = 1.2 nm
Frequency (%)
Particle Size /nm
0
5
10
15
20
25
30
35
0.2
0.4
0.6
0.8
1.0
1.2
1.4
1.6
1.8
2.0

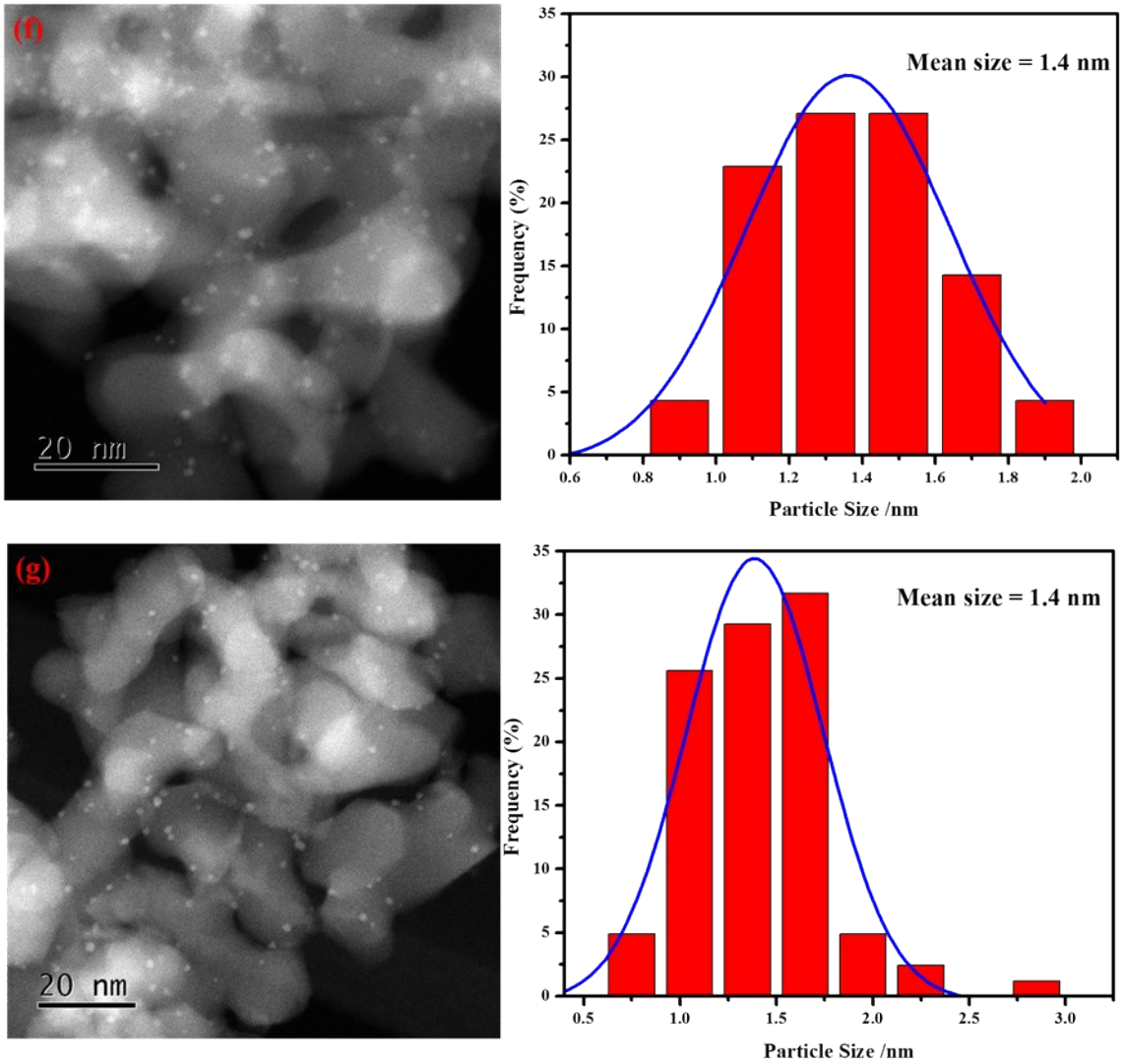

Figure S5 Aberration-corrected HAADF-STEM images of nano-Pt/Fe_2O_3 synthesized by the colloid method.

The HAADF images show that the colloidal Pt particles are uniformly distributed in the as-prepared nano-Pt/Fe_2O_3 catalyst. We did not detect any agglomeration of the colloidal Pt nanoparticles (Figure S5a). High-magnification images (Figure S5b-d) reveals that most of the colloidal Pt particles are single crystals. Some Pt atoms are also observable (indicated by the yellow arrows). As shown in the size distribution plots (Figure S5e-g), the average size of the colloidal Pt particles was estimated to be 1.3 ± 0.1 nm with most of the Pt particles in the size range of 1-2 nm. The number of perimeter Pt atoms were calculated based on the semi-sphere model of the Pt particles without considering the specific shapes and other factors that may affect the estimation. The Pt-Pt bond length is 0.277 nm obtained from the EXAFS data.[1]

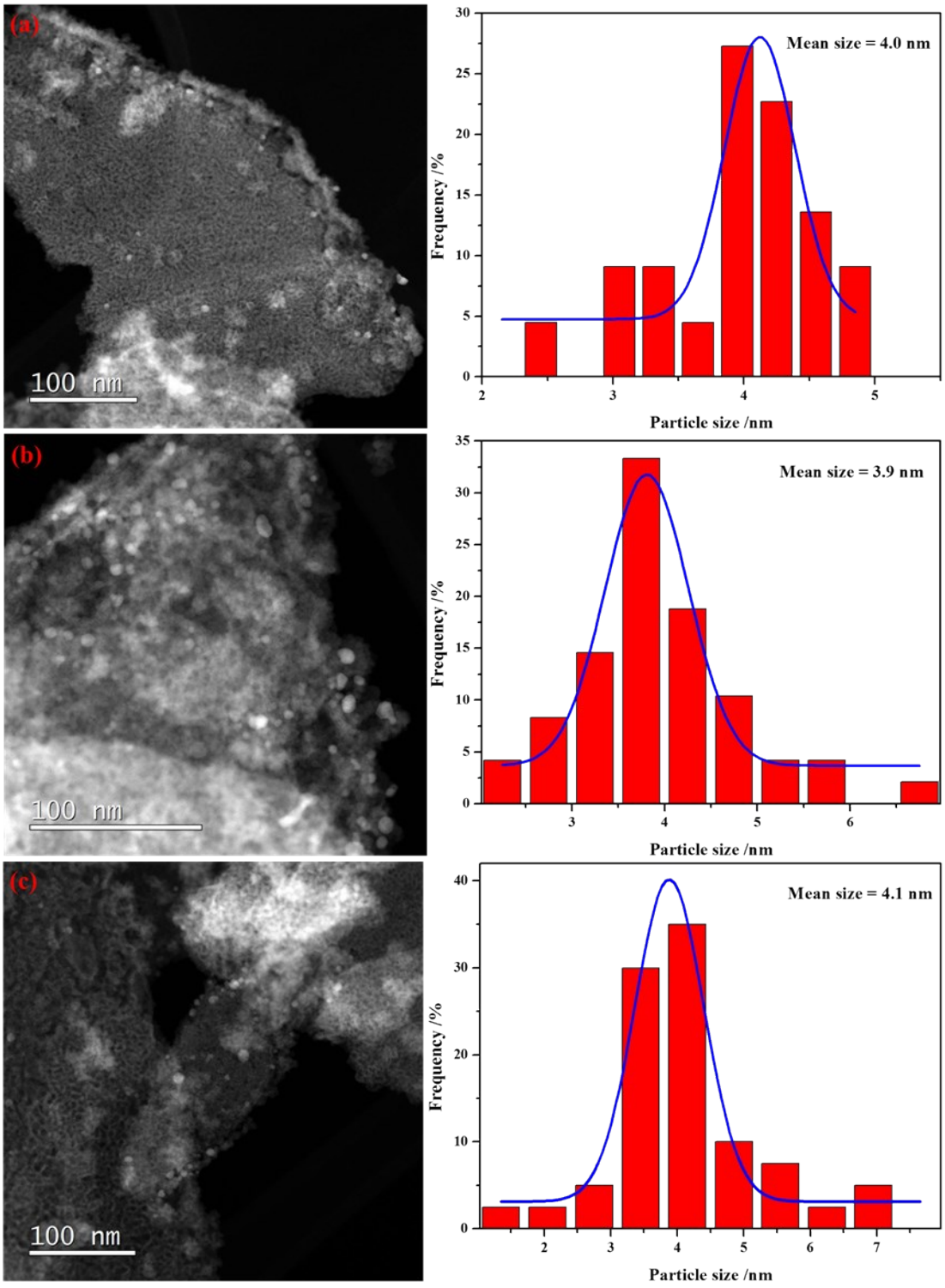
(a)
100 nm
Mean size = 4.0 nm
Frequency /%
Particle size /nm
(b)
100 nm
Mean size = 3.9 nm
Frequency /%
Particle size /nm
(c)
100 nm
Mean size = 4.1 nm
Frequency /%
Particle size /nm

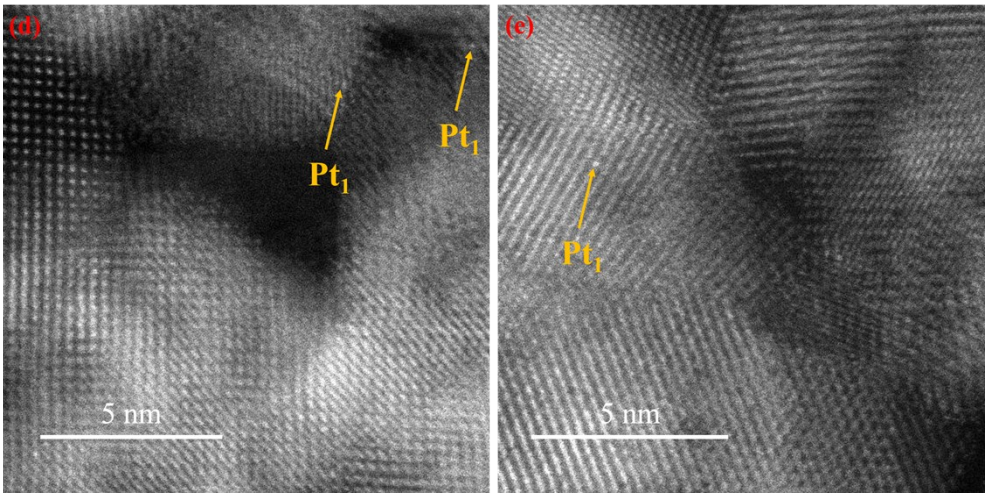

Figure S6 Aberration-corrected HAADF-STEM images of nano-Pt/CeO_2 synthesized by the colloid method.

The HAADF images show that the colloidal Pt particles are uniformly distributed in the as-prepared nano-Pt/CeO_2 catalyst. We did not detect agglomeration of the colloidal Pt nanoparticles. The Pt particle size distribution seems to be wide with the presence of larger Pt particles. Pt_1 atoms were also observed (indicated by the green arrows). The average size of the Pt colloidal particles was estimated to be 4.0 ± 0.1 nm with particle sizes ranging from 1 nm to 7 nm. The number of perimeter Pt atoms were calculated based on the semi-sphere model of the Pt particles without considering the specific shapes and other factors that may affect the estimation. The Pt-Pt bond length is 0.277 nm obtained from the EXAFS data.[1]

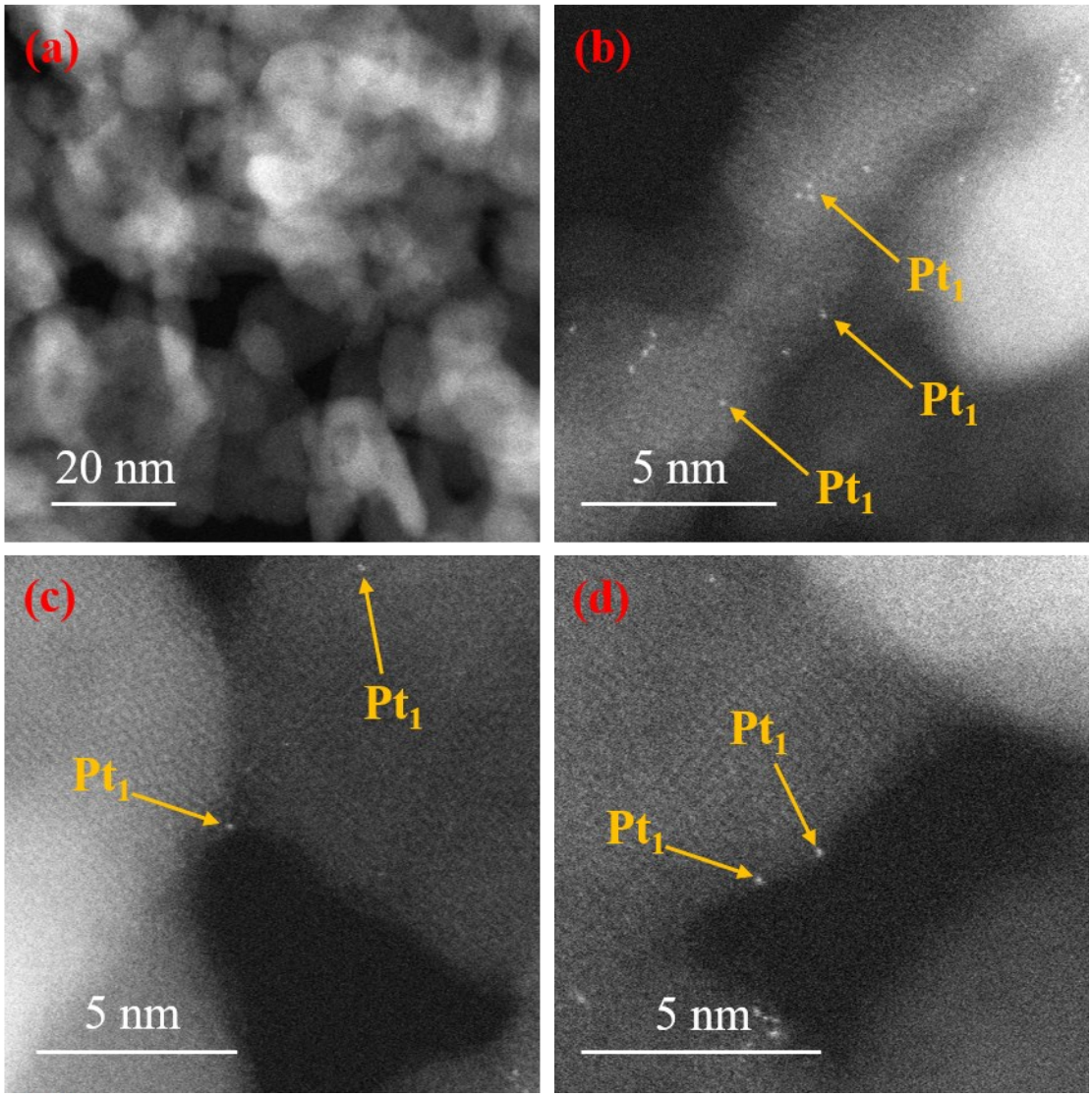

Figure S7 Low-magnification and high-magnification aberration-corrected HAADF-STEM images of fresh $Pt_1/\gamma\text{-}Al_2O_3$ SAC.

As shown in the low-magnification image (a), there are no Pt particles present in the $Pt_1/\gamma\text{-}Al_2O_3$ SAC. High-magnification images (b-d) confirmed the presence of single Pt species. Based on the HAADF-STEM images, we concluded that the as-synthesized $Pt_1/\gamma\text{-}Al_2O_3$ SAC contains only Pt_1 atoms without the presence of any Pt clusters or particles.

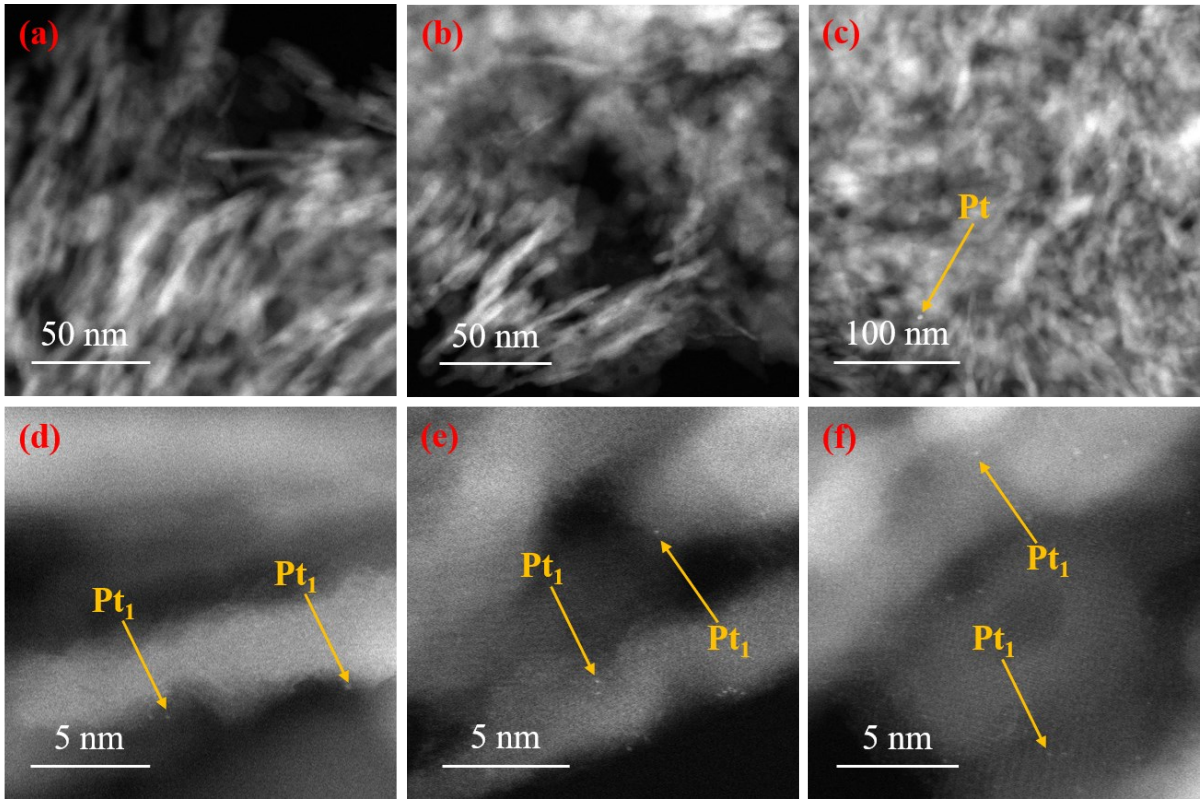

Figure S8 Low-magnification and high-magnification aberration-corrected HAADF-STEM images of used $Pt_1/\gamma\text{-}Al_2O_3$ SAC.

The low-magnification images (a-b) show that most of the regions do not contain any observable Pt clusters or particles. By examining numerous regions of the catalyst few Pt clusters/particles occasionally appear (c), suggesting that sintering of Pt_1 atoms may have occurred during the catalytic reaction. High-magnification images (b-d), however, confirmed that the majority of the Pt species are in the form of single atoms. Based on the HAADF-STEM images, we concluded that the used $Pt_1/\gamma\text{-}Al_2O_3$ SAC mainly contains Pt_1 atoms plus very few Pt clusters.

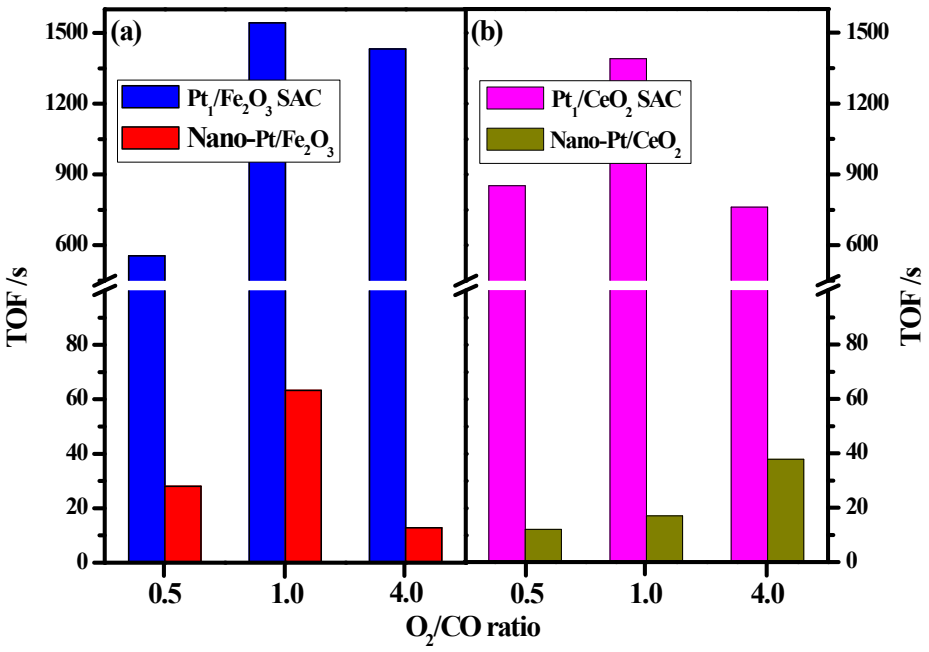

Figure S9 The TOF of Pt_1 atoms and Pt particles of Pt_1/Fe_2O_3 SAC and nano-Pt/Fe_2O_3 (a); Pt_1/CeO_2 SAC and nano-Pt/CeO_2 (b). The TOF was measured in the feed gas of different O_2/CO ratios at 350 °C with the space velocity of 17, 400 l/g•h to 52, 000 l/g•h and pressure = 0.1M Pa: 1) 1.0 vol.% CO, 4.0 vol.% O_2 and He balance (O_2/CO = 4); 2) 2.5 vol.% CO, 2.5 vol.% O_2 and He balance (O_2/CO = 1); 3) 2.5 vol.% CO, 1.25 vol.% O_2 and He balance (O_2/CO = 0.5).

The TOFs of Pt_1 atoms on Pt_1/Fe_2O_3 SAC and Pt_1/CeO_2 SAC are as high as 1542.7/s and 1389.3/s at 350 °C when the O_2/CO volume ratio is adjusted to ~1 (feed gas of 2.5 vol.% CO, 2.5 vol.% O_2 and He balance). When the O_2/CO ratio is increased to 4 (1.0 vol.% CO, 4.0 vol.% O_2 and He balance) or decreased to 0.5 (2.5 vol.% CO, 1.25 vol.% O_2 and He balance), the TOF values change to 1432.7/s and 554.8/s (over Pt_1/Fe_2O_3 SAC), and 852.5/s and 762.1/s (over Pt_1/CeO_2 SAC), respectively. These results clearly demonstrate that the super activity of CO oxidation on the Pt_1 atoms is affected by the gas composition and that the nature of the support plays a major role as well.

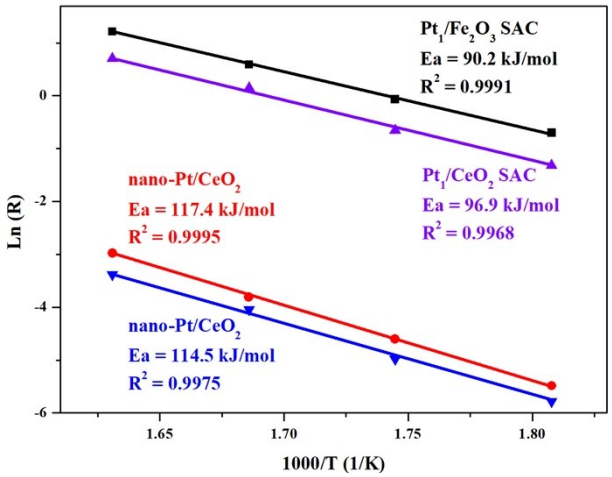

Figure S10 Apparent activation energy (E_a) of CO oxidation over Pt_1/Fe_2O_3 (square symbols), Pt_1/CeO_2 (triangle up symbols), nano-Pt/CeO_2 (triangle down symbols) and nano-Pt/Fe_2O_3 (circle symbols) samples. Arrhenius plots for the reaction rate on these samples in the temperature (T) range of 280 to 320 °C. Feed gas composition: 1 vol.% CO, 4 vol.% O_2 and He balance; space velocity: 9,000 l/g•h ~ 45,000 l/g•h; and Pressure: 0.1 MPa.

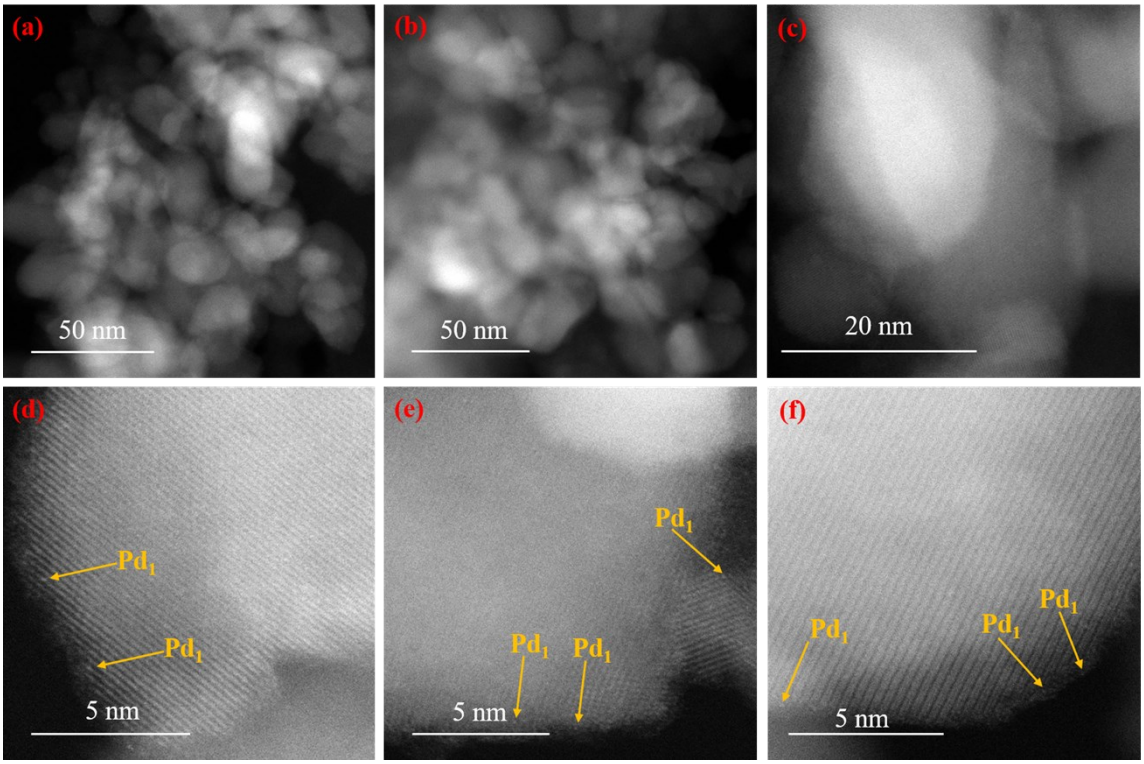

Figure S11 Low-magnification and high-magnification aberration-corrected HAADF-STEM images of used Pd_1/Fe_2O_3.

As shown in the low-magnification images (a-c), there are no Pd particles/clusters present in the used Pd_1/Fe_2O_3 SAC. High-magnification images (d-f) from different regions of the catalyst confirmed the presence of single Pd species after the catalytic reaction. Based on the HAADF-STEM images, we concluded that the Pd_1 atoms did not sinter during the catalytic reaction, which assures that the measured catalytic activity originated from the Pd_1 atoms rather than the Pd clusters or particles.

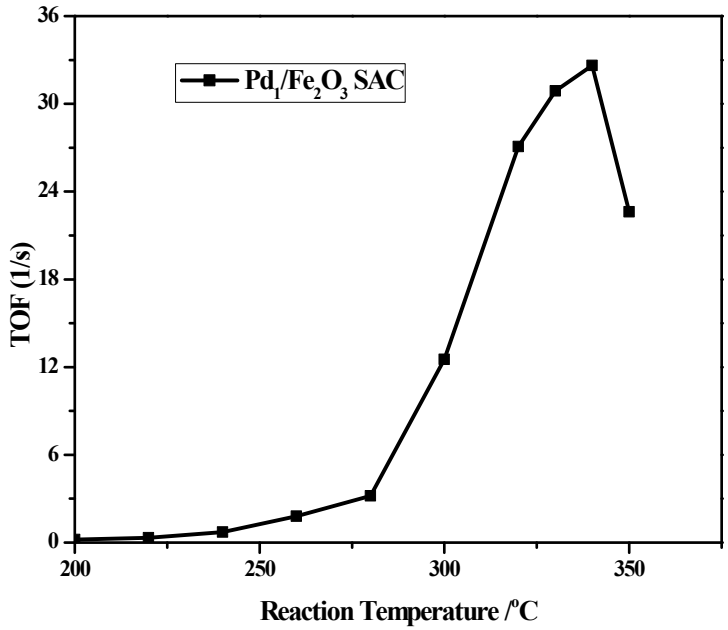

Figure S12 The TOF over Pd_1/Fe_2O_3 SAC for CO oxidation in the temperature range of 200°C to 350°C.

Reaction conditions: 1.0 vol.% CO, 4.0 vol.% O_2 and He balance with the space velocity of 4, 200 l/g • h to 9, 000 l/g • h, pressure = 0.1M Pa.

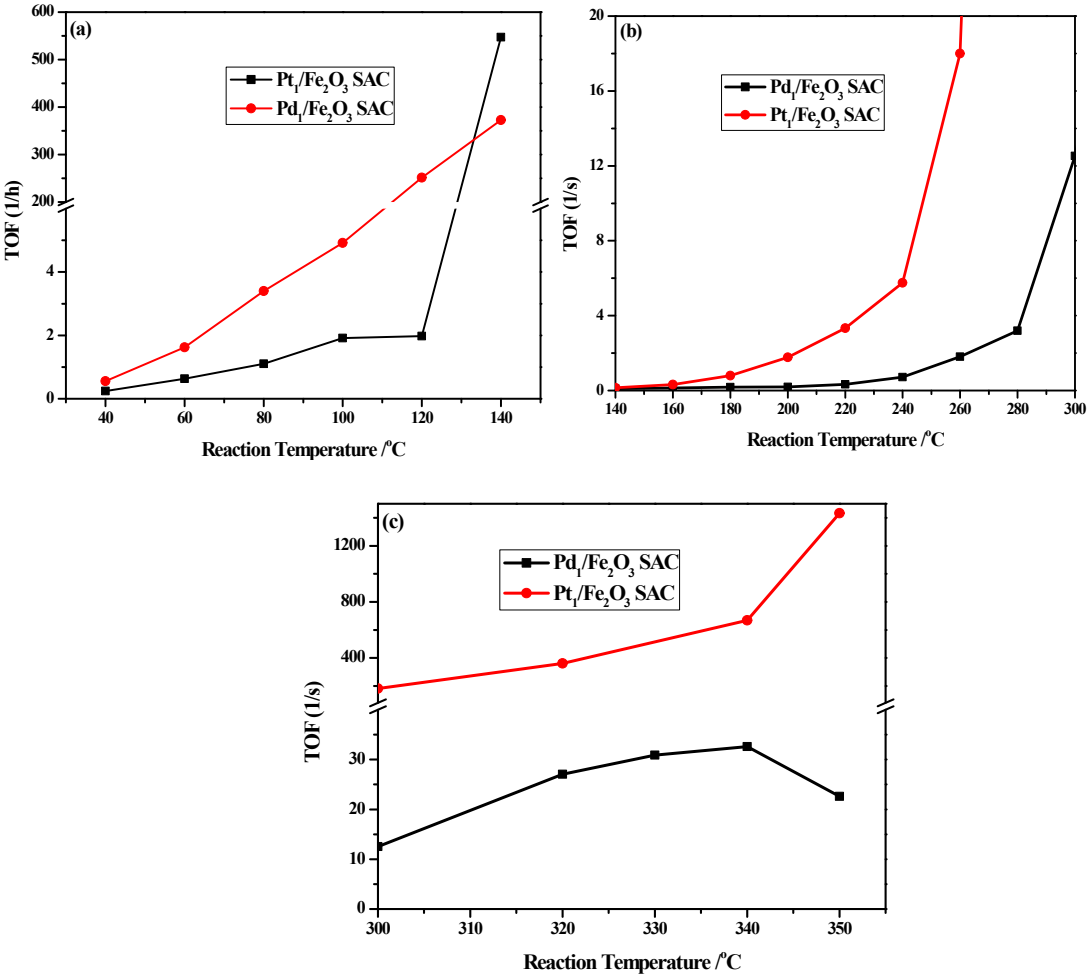

Figure S13 The TOF of Pd_1/Fe_2O_3 and Pt_1/Fe_2O_3 SACs for CO oxidation from 40°C to 140°C (a), 140-300°C (b), and 300-350°C (c). Reaction conditions: 1.0 vol.% CO, 4.0 vol.% O_2 and He balance with the space velocity of 10 l/g • h to 9,000 l/g • h, pressure = 0.1M Pa.

For CO oxidation at low reaction temperatures (40°C to 120°C), the Pd_1/Fe_2O_3 SAC shows much higher activity than that of the Pt_1/Fe_2O_3 SAC as shown in Figure S13a. When the reaction temperature increases to 140 °C or higher (Figure 13 b-c), the TOF of the Pt_1/Fe_2O_3 SAC overtakes that of the Pd_1/Fe_2O_3 SAC and significantly increases at reaction temperatures > 260 °C. It is also interesting to note that the TOF of the Pd_1/Fe_2O_3 SAC reaches a maximum at around 340°C and then decreases with further increase in reaction temperature. The Pt_1/Fe_2O_3 SAC may exhibit a similar behavior at a higher reaction temperature. Such a behavior may be related to the structural changes between the Pt_1 atom and the support surfaces. Further experiments are needed to understand this phenomenon.

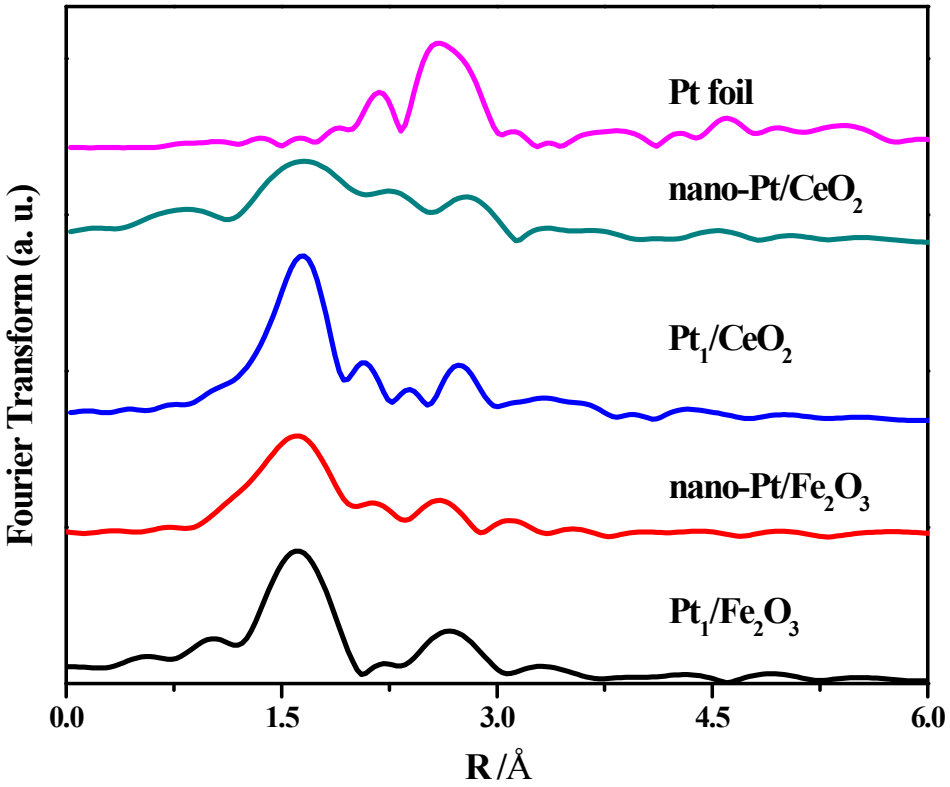

Figure S14 The k^2-weighted Fourier transform spectra derived from the EXAFS on Pt SAC, nano-Pt catalysts and Pt foil; k ranges from 3.0 to 13.9 $Å^{-1}$.

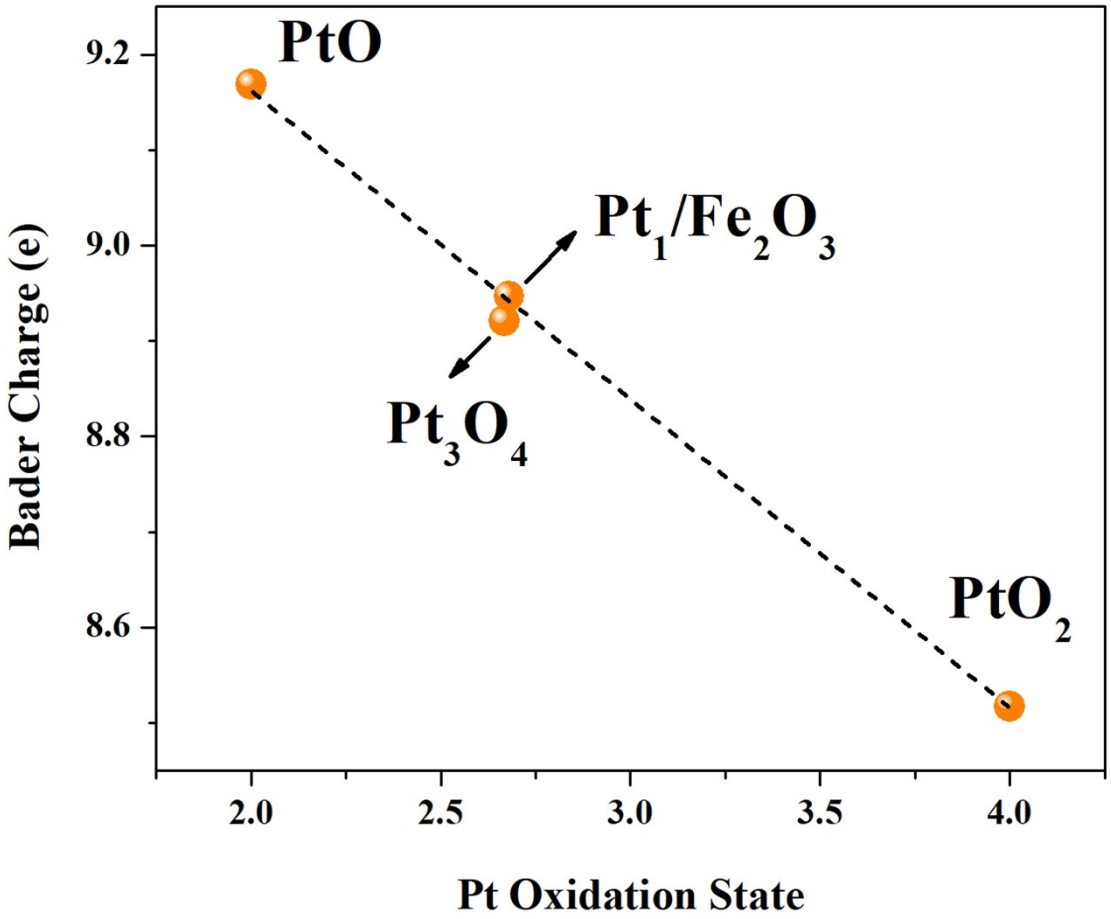

Figure S15 The Bader charge plotted as a function of Pt oxidation state.

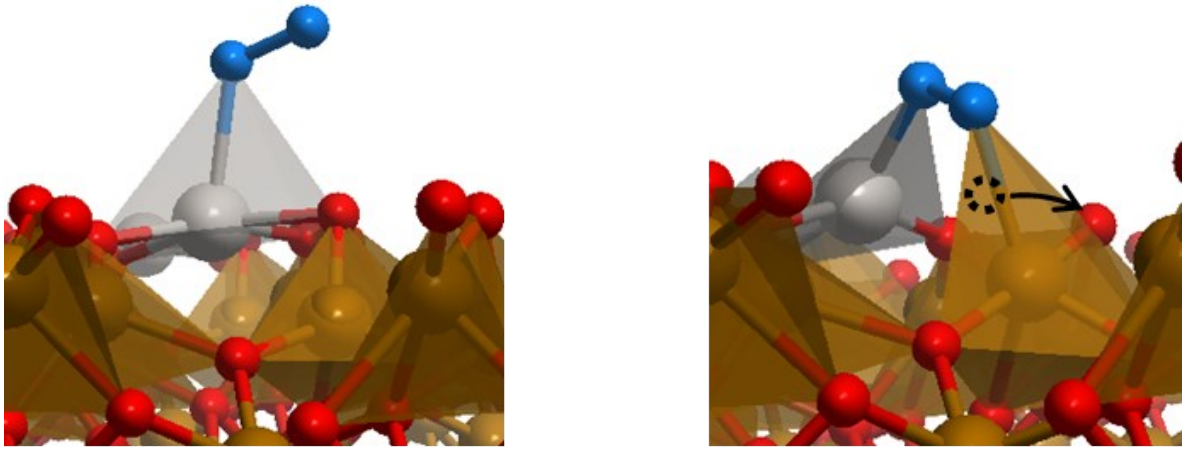

Figure S16 The side-view images of O_2 adsorption configurations corresponding to (ii) and (iii) in Figure 6 in the main manuscript.

Table S1 Specific Reaction Rate of Pt at 350 °C (mmolCO/(g_{Pt}*s))

Samples	Ratio of O_2 to CO[a]		
	4.0	1.0	0.5
Pt_1/Fe_2O_3 SAC	7344.2	7908.3	2844.2
Nano-Pt/Fe_2O_3	39.3	193.2	85.6
Pt_1/CeO_2 SAC	3906.6	7121.5	4370.0
Nano-Pt/CeO_2	79.3	35.7	25.0
Pt/Al_2O_3	/	0.2[b]	/
$Pt/CeO_2/Al_2O_3$	/	1.0[b]	/

a: The specific reaction rates of Pt_1 atoms and Pt particles are measured in the feed gas of 1.0 vol.% CO, 4.0 vol.% O_2 and He balance (O_2/CO=4.0); 2.5 vol.% CO, 2.5 vol.% O_2 and He balance (O_2/CO=1.0); 2.5 vol.% CO, 1.25 vol.% O_2 and He balance (O_2/CO=0.5).

b: The specific reaction rate ratio of Pt is calculated based on the original data shown in Ref. [2] The O_2/CO ratio was 1.1.

Table S2 EXAFS parameters of Pt SACs, nano-Pt catalysts and Pt foil

Sample	Shell	C. N.[a]	R (Å)	$(h_J)_{t,s}$[b]	σ^2
Pt_1/Fe_2O_3	Pt-O	4.4	2.01	0.393	0.00092
	Pt-Pt	/	/		/
Nano-Pt/Fe_2O_3	Pt-O	2.8	2.01	0.365	0.00517
	Pt-Pt	1.9	2.75		0.00528
Pt_1/CeO_2	Pt-O	4.3	2.00	0.389	0.0006
	Pt-Pt	/	/		/
Nano-Pt/CeO_2	Pt-O	3.0	2.01	0.357	0.00867
	Pt-Pt	3.4	2.75		0.00617

a) C. N.: Coordination number.

b) $(h_J)_{t,s}$ is Pt *d*-orbital vacancies per atom. The $(h_J)_{t,s}$ is based on the simplified equation formula.[3-4] The total amount of *d*-band vacancies of Pt in the sample can be evaluated as: $(h_J)_{total,\ sample} = (1.0 + f_d) * (h_J)_{total,\ reference}$; $f_d = (A_{sample}-A_{reference})/(A_{sample}*A_{reference})$, A_{sample} is the Pt L_3 peak area of samples and $A_{reference}$ is the Pt L_3 peak area of Pt foil; The total amount of unoccupied *d*-states for pure Pt has been evaluated from band structure calculation is 0.3.[5-6]

Table S3 Free energy changes (ΔG) of elementary steps during CO oxidation by non-classic MvK mechanism.

Steps	ΔG (eV)
i → ii	-0.03
ii → iii	-0.07
iii → iv	-2.12
iv → iv	-1.14
v → i	-2.68

Reference

1 S. Mukerjee, S. Srinivasan, M. P. Soriaga, J. Mcbreen, Role of structural and electronic-properties of Pt and Pt alloys on electrocatalysis of oxygen reduction - an in-situ XANES and EXAFS investigation. *J Electrochem Soc.* **1995**, 142 (5),1409-1422.

2 M. Ozawa, T. Okouchi, M. Haneda, Three way catalytic activity of thermally degenerated Pt/Al_2O_3 and Pt/CeO_2-ZrO_2 modified Al_2O_3 model catalysts, *Catal Today.* **2015**, 242, 329-337.

3 S. Mukerjee, S. Srinivasan, M. P. Soriaga, J. McBreen, Effect of Preparation Conditions of Pt Alloys on Their Electronic, Structural, and Electrocatalytic Activities for Oxygen Reduction - XRD, XAS, and Electrochemical Studies. *J. Phys. Chem.* **1995**, 99, 4577-4589.

4 A. N. Mansour, J. W. Cook, D. E. Sayers, Quantitative technique for the determination of the number of unoccupied d-electron states in a platinum catalyst using the $L_{2,3}$ X-ray absorption edge spectra. *J. Phys. Chem.* **1984**; 88, 2330-2334.

5 M. Brown, R. E. Peierls, E. A. Stern, White lines in x-ray absorption. *Phys. Rev. B.* **1977**, 15 (2): 738-744.

6 L. F. Mattheiss, R. E. Dietz, Relativistic tight-binding calculation of core-valence transitions in Pt and Au. *Phys. Rev. B.* **1980**, 22 (4), 1663-1676.